Crystallographic controls on the frictional behavior of dry and water-saturated sheet structure minerals

Diane E. Moore and David A. Lockner
U. S. Geological Survey, Menlo Park, California, USA

Received 9 May 2003; revised 2 October 2003; accepted 24 October 2003; published 3 March 2004.

[1] We compare the frictional strengths of 17 sheet structure mineral powders, measured under dry and water-saturated conditions, to identify the factors that cause many of them to be relatively weak. The dry coefficient of friction μ ranges upward from 0.2 for graphite, leveling off at 0.8 for margarite, clintonite, gibbsite, kaolinite, and lizardite. The values of μ (dry) correlate directly with calculated (001) interlayer bond strengths of the minerals. This correlation occurs because shear becomes localized along boundary and Riedel shears and the platy minerals in them rotate into alignment with the shear planes. For those gouges with μ (dry) < 0.8, shear occurs by breaking the interlayer bonds to form new cleavage surfaces. Where μ (dry) = 0.8, consistent with Byerlee's law, the interlayer bonds are sufficiently strong that other frictional processes dominate. The transition in dry friction mechanisms corresponds to calculated surface energies of 2–3 J/m^2. Adding water causes μ to decrease for every mineral tested except graphite. If the minerals are separated into groups with similar crystal structures, μ (wet) increases with increasing interlayer bond strength within each group. This relationship also holds for the swelling clay montmorillonite, whose water-saturated strength is consistent with the strengths of nonswelling clays of similar crystal structure. Water in the saturated gouges forms thin, structured films between the plate surfaces. The polar water molecules are bonded to the plate surfaces in proportion to the mineral's surface energy, and μ (wet) reflects the stresses required to shear through the water films. *INDEX TERMS:* 3947 Mineral Physics: Surfaces and interfaces; 3999 Mineral Physics: General or miscellaneous; 5199 Physical Properties of Rocks: General or miscellaneous; *KEYWORDS:* frictional strength, fault gouge, sheet silicates

Citation: Moore, D. E., and D. A. Lockner (2004), Crystallographic controls on the frictional behavior of dry and water-saturated sheet structure minerals, *J. Geophys. Res.*, *109*, B03401, doi:10.1029/2003JB002582.

1. Introduction

[2] In compiling the available friction data on rocks and rock-forming minerals, *Byerlee* [1978] found that the maximum coefficient of friction, μ typically had a value of $\approx$0.85 at normal stresses $\leq$200 MPa. This value has come to be known as Byerlee's law. This simple rule for estimating frictional resistance has been found to apply in laboratory experiments to effective stress such that $\mu = \tau/\sigma_n'$, where τ is shear stress, $\sigma_n' = (\sigma_n - Pp)$ is effective normal stress, and Pp is pore pressure. However, one group of minerals, the sheet silicates, provides a major exception to Byerlee's law. These layer-structure minerals vary in strength, but the most common ones have coefficients of friction in the range 0.2–0.5 under water-saturated conditions. Concentrations of such weak minerals in an active fault zone potentially could exert a major influence on the fault's behavior, but we need to understand what controls the strength of these minerals in order to accurately predict their behavior at seismogenic depths.

[3] As part of our investigations of the frictional strength of serpentine minerals [*Moore et al.*, 1996b, 1997], we found that thoroughly dried serpentine-gouge samples have coefficients of friction consistent with Byerlee's law. The results for serpentine led us to test whether other layer-structure minerals, including nonsilicates, would be equally strong under dry conditions. Of our initial sample set, only dry kaolinite was as strong as dry serpentine, the other dry values of μ ranging down to a minimum of 0.18 for graphite [*Morrow et al.*, 2000]. Significantly, though, the range of μ (dry) showed a possible correlation with the calculated (001), or interlayer, bond strengths of the minerals [*Giese*, 1978, 1980; *Bish and Giese*, 1981].

[4] In this paper, we confirm the relationship between interlayer bond strength and dry frictional strength for sheet structure minerals and present petrographic data that illustrate why this correlation exists. Further, the expanded data set has revealed a relationship between water-saturated strength and some of the factors that contribute to interlayer bonding, although the controls on wet friction for these minerals are more complex than those for dry friction. These results emphasize the pronounced crystallographic influences on the frictional properties of sheet structure minerals. In turn, crystallographic control of friction pre-

0148-0227/04/2003JB002582$09.00

dicts which of these minerals will, and which ones will not, be weak at several kilometers depth within a fault zone.

2. Experiments

2.1. Minerals Tested

[5] Over the course of this investigation we ran experiments on 17 synthetic gouge materials made up of different mineral separates, including the native elemental carbon, graphite, two hydroxide minerals, and several 1:1 and 2:1 sheet silicates (Figure 1). Sample descriptions are presented in Appendix A. An effort was made to obtain both dioctahedral and trioctahedral examples of a given crystal structure (Figure 1), and in the case of the flexible micas, three separates of each type were prepared to test the effects of mineral composition and layer stacking sequence on frictional strength.

[6] The talc and graphite starting materials are pure commercial powders, and no chemical analysis of either one was made. The montmorillonite was also obtained commercially, and its composition was provided by the company (Appendix A). The other 14 samples (15 minerals, one sample is a mixture of paragonite + muscovite) were prepared from natural mineral or rock specimens, and their compositions were determined using electron microprobe techniques. Twelve mineral compositions are listed in Table 1; each one represents an average of 20–24 spot analyses. Kaolinite, brucite, and gibbsite have nearly end-member compositions (Figure 1) and were left out of Table 1. The kaolinite contains ≈0.25 wt % FeO and 0.30% TiO_2, the brucite contains ≈0.25 wt % each FeO and MnO, and the gibbsite contains ≈0.50 wt % each SiO_2 and F.

[7] Mineral separates were prepared by handpicking crystals from the rock and mineral specimens with the aid of a stereomicroscope. Some of the micas were large crystals, and separation merely involved the removal of weathered areas or coatings on cleavage surfaces. Polycrystalline rock samples were broken into small enough pieces that individual crystals could be extracted. The paragonite + muscovite sample came from a fine-grained schist, and it was impossible to distinguish the two minerals visually. Because they have the same crystal structure (Figure 1), the mixed separate was included in the sample set. Each mineral separate was hand ground and passed through a 90-μm sieve to produce a synthetic gouge. Combined X-ray diffraction, thin section, and scanning electron microscopy (SEM) investigations attest to the scarcity of impurities in the mineral separates.

2.2. Procedures

[8] The experimental procedures are nearly the same as those used by *Morrow et al.* [2000]. An initially 1.1-mm-thick layer of a given gouge was placed between 25.4-mm-diameter cylindrical driving blocks containing a 30° saw cut (Figure 2). The upper driving block was composed of Berea sandstone, and the lower block was Westerly granite. Both saw cut surfaces were ground with 220-grit SiC. *Morrow et al.* [2000] had used impermeable, fused silica for the lower block, considering that pore fluids might become trapped in a more porous material and generate excess fluid pressures due to poroelastic effects during shear. However, replacing the fused silica with low-permeability Westerly granite has no effect on the measured water-saturated strengths, as described in the next section, and the granite blocks are much easier to prepare and handle. The gouge layer was applied to the granite saw cut as a thick slurry, and the sandstone block was placed over the gouge layer. The sample was inserted into a 0.05-mm-thick copper sleeve to keep the assembly intact and vacuum-dried at 120°C overnight (generally for a 22-hour period). The copper sleeve ruptures during the initial 1–2 mm of axial displacement and therefore does not contribute to the reported shear strengths. The 120°C drying temperature was chosen, because differential thermal analyses of many clays indicate that adsorbed water is removed at temperatures slightly above 100°C [*Mackenzie*, 1957; *Deer et al.*, 1962]. To minimize the possibility of contamination with room humidity, the sample was removed from the vacuum oven while still warm, and placed in a polyurethane jacket that was immediately clamped to the steel end plugs (Figure 2). The transfer of the sample from the vacuum oven to the pressure vessel was accomplished in a few minutes. The sample assembly and the pore pressure lines were evacuated for 20–25 min, after which the sample was isolated from the rest of the pore pressure system during the dry portion of the experiment.

[9] Confining pressure of 100 MPa was applied to the sample, which was sheared dry to 4-mm axial displacement at 100 MPa constant normal stress and 0.5-μm/s axial displacement rate. The normal stress was maintained at a constant value by means of computer-controlled adjustments to the confining pressure. Shear stress was then reduced by backing off the ram 0.1 mm, and deionized water was introduced to a pressure of 10 MPa. The saturated sample was allowed to equilibrate for 60 min, then sliding was resumed at 100 MPa effective normal stress (110 MPa normal stress) to 9-mm axial displacement. We used the procedure outlined by *Stanchits et al.* [2003] to calculate the time needed for the water front to migrate across the gouge layer, using a porosity of 6% and permeability perpendicular to the gouge layer of $1 \times 10^{-19.2}$ m^2, as reported by *Zhang et al.* [2001] for a muscovite gouge subjected to 5-mm shear displacement at 100-MPa effective normal stress. The amount of compaction of the gouge layer varies from sample to sample, but the most commonly measured thicknesses were between 0.5 and 0.6 mm. A 0.6-mm-wide gouge layer should become fully saturated after 28.5 min, slightly less than half the allotted equilibration time.

[10] For samples that showed significant strain hardening while sheared dry, additional all-dry experiments were conducted to determine the peak dry frictional strength. The all-dry samples also were important for the petrographic studies. A few additional experiments were run entirely under water-saturated conditions, employing the same sample-preparation procedures as for the dry/wet experiments. The experimental samples selected for SEM study were cut out of the jackets, and the sandstone and granite forcing blocks were separated to expose the gouge. Following an initial examination with a stereomicroscope, small fragments of gouge were mounted on circular holders for SEM examination. Standard, covered thin sections were prepared from all the remaining samples.

3. Results

3.1. Friction Experiments

[11] We ran repeat experiments on four samples from the previous study. The old and new results for brucite and

Native Element

Mineral	Ideal Formula Unit	Comments
Graphite	C	Layers are held together solely by van der Waals forces.

Hydroxides

A layer consists of a plane of cations sandwiched between two planes of hydroxyl ions. Dipole-dipole bonds form between the hydroxyls in adjacent layers.

Mineral	Ideal Formula Unit	Comments
Brucite	$Mg(OH)_2$	Trioctahedral[a]
Gibbsite	$Al(OH)_3$	Dioctahedral[b]

1:1 Sheet Silicates

A layer consists of a sheet of linked silica tetrahedra attached to an octahedral sheet through shared anion sites. Hydrogens at the top of the octahedral sheet form long hydrogen bonds with the oxygens at the base of the tetrahedral sheet in the next layer.

Mineral	Ideal Formula Unit	Comments
Lizardite	$Mg_3Si_2O_5(OH)_4$	Trioctahedral
Kaolinite	$Al_2Si_2O_5(OH)_4$	Dioctahedral

2:1 Sheet Silicates

A layer consists of an octahedral sheet sandwiched between two tetrahedral sheets. Bonding between layers varies with the amount of cation substitution, which can create a layer charge.

Mineral	Ideal Formula Unit	Comments
No substitution; two tetrahedral sheets face each other across the interlayer, and bonding between them consists mostly of van der Waals forces with a minor electrostatic component:		
Talc	$Mg_3Si_4O_{10}(OH)_2$	Trioctahedral
Pyrophyllite	$Al_2Si_4O_{10}(OH)_2$	Dioctahedral
Smectite clays have minor substitution in either the tetrahedral or octahedral sheet, which is balanced by the addition of interlayer cations:		
Montmorillonite	$(0.5Ca,Na)_{0.33}(Al_{1.67}Mg_{0.33})Si_4O_{10}(OH)_2.nH_2O$	Dioctahedral Octahedral substitution
One of four Si is replaced by Al (true micas). Charge is balanced by adding one monovalent interlayer cation:		
Phlogopite/Biotite	$K(Mg,Fe)_3(Si_3Al)O_{10}(OH)_2$	Trioctahedral
Muscovite	$KAl_2(Si_3Al)O_{10}(OH)_2$	Dioctahedral
Paragonite	$NaAl_2(Si_3Al)O_{10}(OH)_2$	Dioctahedral
Two of four Si are replaced by Al (brittle micas). Charge is balanced by adding one divalent interlayer cation:		
Clintonite	$Ca(Mg_{2.25}Al_{0.75})(Si_{1.25}Al_{2.75})O_{10}(OH)_2$	Trioctahedral Additional Al/Si exchange is balanced by Al/Mg exchange.
Margarite	$CaAl_2(Si_2Al_2)O_{10}(OH)_2$	Dioctahedral
The interlayer contains an entire octahedral sheet:		
Chlorite	$(Mg,Fe,Al)_6(Si,Al)_4O_{10}(OH)_8$	Usually Trioctahedral

[a]All octahedral cation sites are filled with divalent cations.
[b]Two-thirds of the octahedral cation sites are filled with trivalent cations; the other third are vacant.

Figure 1. Sheet structure types tested in this investigation.

Table 1. Microprobe Analyses of Some of Minerals Tested[a]

	True Micas						
	Dioctahedral				Trioctahedral		
	Muscovite I	Muscovite II	Paragonite	Muscovite	Biotite	Phlogopite I	Phlogopite II
SiO_2	45.77	45.78	45.37	46.28	41.25	40.75	36.18
TiO_2	NA	0.09	NA	NA	2.26	0.53	NA
Al_2O_3	32.16	35.18	39.17	33.01	11.29	14.35	18.66
FeO*	3.93	2.64	0.80	2.70	10.97	1.83	3.45
MgO	1.28	0.35	0.06	1.18	18.95	26.28	23.47
MnO	NA	0.06	NA	NA	0.24	0.03	NA
CaO	0.02	–	0.52	–	–	–	0.02
Na_2O	0.53	0.69	6.25	1.57	0.44	0.29	0.32
K_2O	10.67	10.52	1.04	8.84	9.99	10.62	10.05
Cr_2O_3	NA	0.01	NA	NA	0.01	–	NA
Total	94.36	95.32	93.21	93.58	95.40	94.68	92.15
F, wt %	1.50	0.81	0.08	0.14	4.71	4.11	0.50
Si	3.13	3.07	2.97	3.14	3.02	2.89	2.66
Al^{IV}	0.87	0.93	1.03	0.86	0.98	1.11	1.34
Al^{VI}	1.72	1.85	1.99	1.78	–	0.09	0.27
Ti	NA	0.01	NA	NA	0.12	0.02	NA
Fe*	0.22	0.15	0.04	0.15	0.67	0.11	0.21
Mg	0.13	0.03	0.01	0.12	2.07	2.77	2.56
Mn	NA	–	NA	NA	0.01	–	NA
Ca	–	–	0.04	–	–	–	–
Na	0.07	0.09	0.80	0.21	0.06	0.04	0.05
K	0.93	0.90	0.08	0.77	0.94	0.96	0.94
O Anhydrous	11	11	11	11	11	11	11

	Brittle Micas		Other 2:1 Minerals		1:1 Mineral
	Dioctahedral Margarite	Trioctahedral Clintonite	Dioctahedral Pyrophyllite	Chlorite	Trioctahedral Lizardite[b]
SiO_2	30.38	18.11	66.03	25.84	40.32
TiO_2	NA	NA	0.01	0.07	0.02
Al_2O_3	50.00	40.24	28.25	21.62	2.14
FeO*	0.76	3.90	0.20	21.56	6.38
MgO	0.46	21.07	0.01	18.33	35.47
MnO	NA	NA	0.01	0.09	0.07
CaO	10.55	13.14	0.01	0.02	0.04
Na_2O	1.68	0.02	0.05	0.02	NA
K_2O	0.01	–	0.01	–	NA
Cr_2O_3	NA	NA	NA	0.06	0.29
Total	93.84	96.48	94.58	87.61	85.09
F, wt %	0.05	0.08	NA	0.08	NA
Si	2.04	1.28	3.99	2.67	1.98
Al^{IV}	1.96	2.72	0.01	1.33	0.02
Al^{VI}	2.02	0.62	2.00	1.30	0.11
Ti	NA	NA	–	–	–
Fe*	0.04	0.23	0.01	1.87	0.26
Mg	0.04	2.21	–	2.83	2.58
Mn	NA	NA	–	0.01	–
Ca	0.76	0.99	–	–	–
Na	0.22	–	–	–	NA
K	–	–	–	–	NA
O anhydrous	11	11	11	14	7

[a]NA stands for not analyzed. Asterisk indicates total Fe reported as FeO.
[b]Average of compositions is reported by *Moore et al.* [1996a] for a 3:1 ratio of mesh:bastite lizardite, includes 0.36 wt % NiO.

graphite (Figure 3) are nearly identical, including the stick-slip behavior of dry brucite and the peak in dry graphite strength at small displacement. The change from dry to water-saturated conditions has essentially no effect on the strength of graphite gouge, and $\mu = 0.18$ at 9-mm axial displacement. The repeat test on muscovite I (the muscovite of *Morrow et al.* [2000]), which is included with the other micas in Figure 4a, also yielded the same strengths as reported previously. However, the fourth repeat experiment, conducted on talc (Figure 4b), gave a higher dry strength than that reported by *Morrow et al.* [2000]. Because of this discrepancy, we ran an additional, all-dry talc experiment and obtained μ (dry) = 0.36 at 9-mm axial displacement, well above the value of μ (dry) = 0.24 obtained previously. The talc sample tested by *Morrow et al.* [2000] may have been exposed to room humidity, causing μ (dry) to be close to the water-saturated value.

[12] The dioctahedral flexible micas, muscovite and paragonite, have consistently higher values of μ, both dry and wet, than their trioctahedral equivalents, phlogopite and biotite (Figure 4a). Compositional variations within a group, such as the wide range of F and Fe contents among the trioctahedral micas (Table 1) and the mix of Na- and K-bearing dioctahedral micas in one sample, do not signif-

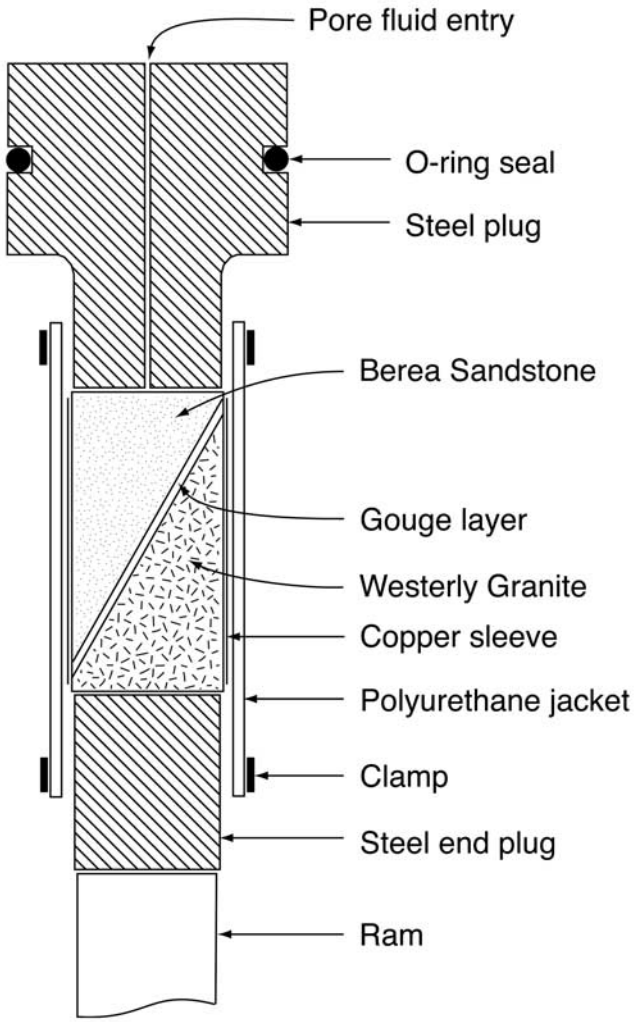

Figure 2. Experimental apparatus.

icantly affect strength. Dry $\mu \geq 0.8$ for the brittle mica margarite is comparable to dry μ values of kaolinite and lizardite, and μ (dry) of clintonite reaches 0.74 at 4-mm displacement. Under water-saturated ("wet") conditions, margarite and clintonite are the strongest of all the minerals tested in this study, with μ (wet) = 0.68–0.70.

[13] The phlogopite I gouge experiments plotted in Figure 5a illustrate the general reproducibility of the dry/wet experiments with separate all-dry and all-wet experiments. The wholly dry and water-saturated experiments reach steady state after 4- to 5-mm axial displacement, and subsequent rates of change of μ with increasing displacement are closely comparable. The early period of dry shear in the dry/wet experiment does not affect the water-saturated frictional strength. The dry and wet gouges take different paths to reach steady state shear, the dry gouge being characterized by progressively slower rates of increase of μ and the water-saturated gouge by a broad, low peak in μ at small displacements. The behavior of these gouges prior to the establishment of steady state shear will vary with the sample preparation and assembly techniques used and whether or not the sample was precompacted at higher stresses than tested in the experiment, among other factors.

[14] Pyrophyllite and talc form another dioctahedral-trioctahedral pair (Figure 1), and the difference in μ between water-saturated pyrophyllite and talc (Figure 4b) is about the same as the difference between the muscovite and phlogopite groups (Figure 4a). Further study is needed to verify μ (dry) of pyrophyllite. The yield point of dry pyrophyllite occurred at $\mu \approx 0.2$, about the same as for talc (Figure 4b), but μ of pyrophyllite continued to increase rapidly with displacement to 4 mm. Additional, all-dry experiments on pyrophyllite (Figure 5b) yielded conflicting results. In one case, μ reached a peak value at ≈4-mm displacement, then declined to a value close to that of dry talc. In two additional experiments, one of them using granite forcing blocks on both sides of the gouge layer, μ increased continuously to ≈0.7 at 9-mm axial displacement. The weaker all-dry sample potentially could have been contaminated with room humidity, but there was no problem with the experimental procedure that would support this possibility. The reproducibility of the strength data for the dry-sheared pyrophyllite samples is much lower than was found for the other gouges (e.g., Figure 5a).

3.2. Gouge Textures

[15] All of the examined gouge layers are characterized by localized shear along boundary and numerous thin Riedel (R) shear planes. A boundary shear typically forms near but not directly on the granite saw cut surface, so that a thin film of gouge covers that surface. The surface of the sandstone forcing block is rougher than that of the granite, and the sandstone-side boundary shear develops adjacent to the sand grains that project farthest into the gouge layer. There was no evidence that any sand grains had been dislodged from the saw cut surfaces and incorporated into the gouge layers.

[16] The appearance of the shear planes varies with the strength of the samples. Boundary shears in the brittle-mica gouges are relatively dull and grainy (Figure 6a). With decreasing strength of the gouge the boundary shears become increasingly smooth and shiny, with graphite (Figure 6b) and talc having very reflective surfaces. Boundary-shear planes are characterized by corrugations or slickensides that are aligned in the direction of shear, and a finer-scale set of striae usually is superposed on the coarser set (see also Figures 8d and 8e of *Moore et al.* [1997] for similar structures in serpentine gouges). The larger-scale corrugations in one all-dry talc sample (Figure 6c) have wavelengths on the order of 50 μm, and the finer-scale striae have wavelengths of about 5 μm. The R shears are more irregular than the boundary shears, but they too are striated (Figure 6b). Individual R shears do not span the width of a sample, but they generally occur in groups of 4 or 5 closely spaced shears that together cross the sample.

[17] Both the boundary and R shears are characterized by the strong alignment of the platy grains roughly parallel to the shear surfaces (Figure 6d). The alignment of plates is especially well developed in the weaker samples, whereas in the stronger samples this preferred orientation is obscured under a cover of very fine grained, equigranular fragments (Figure 6e). Figure 6f shows a single phlogopite grain in a boundary shear that has a stair-step arrangement of the layers on one side, suggestive of small offsets along the (001) cleavage.

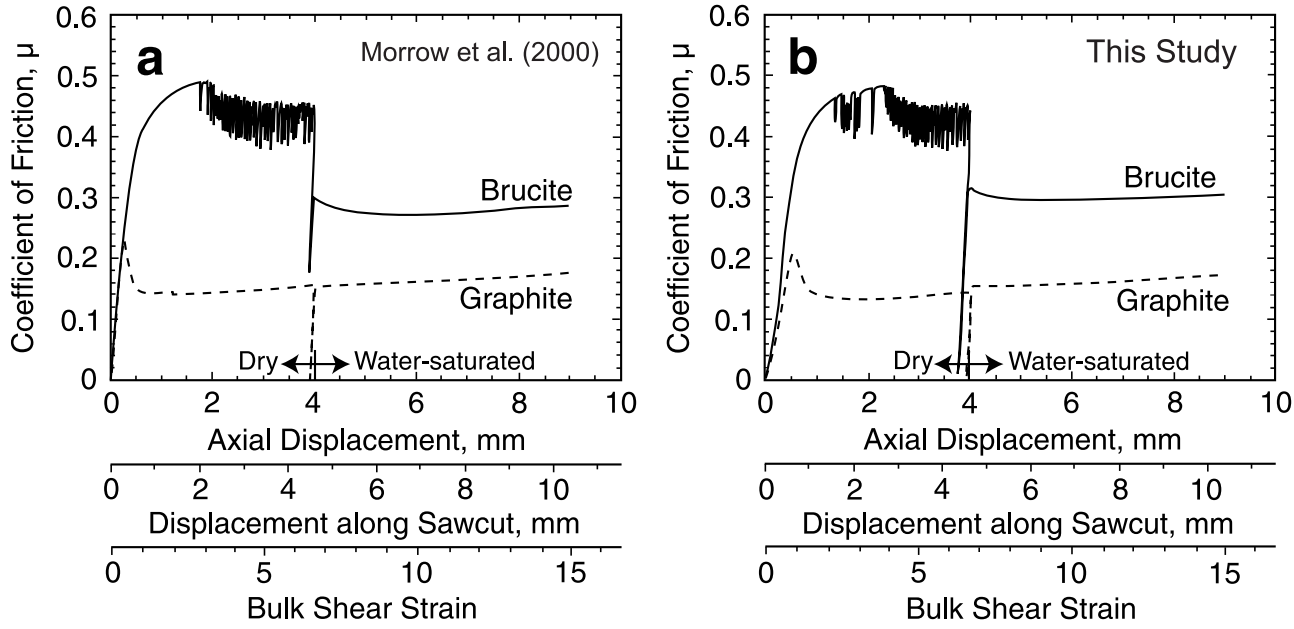

Figure 3. Comparison of duplicate experiments on brucite and graphite from (a) *Morrow et al.* [2000] and (b) this study. Conditions are as follows: 100 MPa normal stress, dry 0- to 4-mm axial displacement, followed by 110 MPa normal stress, 10 MPa fluid pressure at 4-to9-mm axial displacement. The two additional horizontal scales resolve the displacement along the saw cut surface and estimate the bulk shear strain assuming a 0.6-mm-thick compacted gouge (see text).

[18] The gouge between shears is grouped into numerous small domains of aligned crystals. The preferred orientation varies widely from domain to domain, but on average the trend is in the opposite direction to that of the R shears ("P fabric" [e.g., *Moore et al.*, 1989]), as viewed in thin section. The modest fabric in the bulk of the gouge layer may have been initiated during sample assembly and subsequently rotated in response to offset along the shear surfaces. It contrasts markedly to the strong preferred alignment within the shear planes. Such textural contrasts are commonly observed in phyllosilicate-rich gouges that are sheared in laboratory tests [e.g., *Moore et al.*, 1989, 1997], and they may be associated with substantial permeability anisotropies [*Zhang et al.*, 2001].

[19] Flakes of biotite from the Westerly granite saw cut surface have been incorporated into some of the gouge layers and smeared out in the direction of shear to form black streaks (Figure 7a). Several of the biotite streaks cross the gouge layer along R shears and then continue along the sandstone-side boundary shear. At low magnifications the outlines of streaks are readily identifiable in secondary-electron SEM images (Figure 7b); at higher magnifications the streaks show the same alignment of platy grains as other parts of the shear. Some of these biotites have been so strongly thinned that the streaks are nearly colorless in places.

[20] The biotite streaks are found only in those gouge layers for which μ (dry) of the gouge $\geq \mu$ (dry) of biotite. Thus the margarite, clintonite, gibbsite, muscovite and phlogopite samples (Figure 4) contain biotite streaks, whereas the talc, graphite, and brucite samples do not. The maximum length of the streaks in a given sample varies with the type of experiment conducted. The longest streaks in dry/wet samples are 4–5 mm, whereas streaks up to 10 mm in length are present in samples sheared dry to 9-mm axial displacement, which corresponds to 10.4-mm displacement along the saw cut. Other gouge materials with μ (dry) <0.8 also form streaks, but they are less obvious than the biotite streaks because of the lack of color contrast.

[21] The textures of the pyrophyllite samples vary with their strength (Figure 5). The dry/wet sample and the weaker all-dry sample have the smooth, shiny shear planes (Figure 8a) that are characteristic of the weaker gouges, whereas the shears in the strong all-dry samples are dull, grainy, and very rough (Figure 8b). The stronger dry samples contain isolated patches of oriented pyrophyllite grains embedded in the unoriented gouge (Figure 8c). At high magnifications the platy minerals at shear surfaces (Figure 8d) show a range of orientations from parallel to perpendicular to the shear planes, and some of the grains appear to contain kink bands.

4. Discussion

4.1. Dry Friction

[22] *Giese* [1973, 1974, 1975a, 1978, 1980] and *Bish and Giese* [1981] calculated the changes in electrostatic energy, expressed as surface energies in units of kcal/mol, accompanying separation of the layers along the (001) plane of a wide range of layer-structure minerals. The electrostatic or Coulomb attraction forms only one part of the total lattice energy of a crystal, the other two parts being a van der Waals attractive force and a repulsion term that is of opposite sign and probably similar size to the van der Waals force. The Coulomb energy also contributes to the lattice energy over a greater distance than the other two terms. Because of these factors the difference in electrostatic energy between a normal and separated structure should

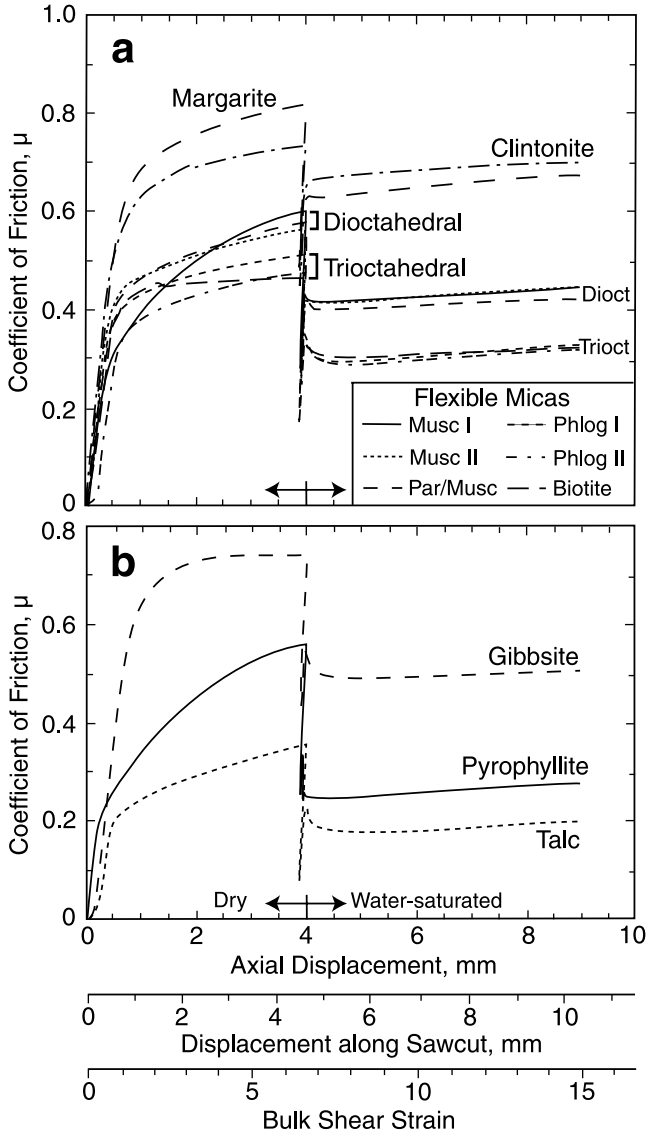

Figure 4. Friction data from dry/wet experiments on (a) six flexible micas and the brittle micas margarite and clintonite and (b) gibbsite, pyrophyllite, and talc. Horizontal axes are the same as in Figure 3.

provide a reasonable approximation to the interlayer bonding energy [*Giese*, 1975b].

[23] *Giese* [1978] found that the strongest interlayer bonds are those of the brittle micas, which have a large layer charge that is balanced by the addition of a divalent interlayer cation. The 1:1 sheet silicates (Figure 1), in which the layers are held together by hydrogen bonds, are also relatively strong. The weakest bonds are found in the two neutral-layer 2:1 structures, talc and pyrophyllite, but *Giese* [1975a] emphasized that the calculated electrostatic energies for both minerals are not small compared to their van der Waals energies. A dioctahedral mineral always has stronger interlayer bonds than its trioctahedral counterpart [*Giese*, 1978], despite variations in composition or layer stacking sequence. Because of differences in hydroxyl orientations in trioctahedral and dioctahedral micas, substitution of F for OH increases the (001) bond strength of trioctahedral phlogopite by about 25% but has little effect on dioctahedral muscovite. Even so, the 27 kcal/mol interlayer bond energy of F-phlogopite is lower than the corresponding 32 kcal/mol bond strength of muscovite [*Giese*, 1975b]. Similarly, the weakest stacking sequence in muscovite is about 5 kcal/mol stronger than the strongest phlogopite stacking order [*Giese*, 1977]. The origin of the consistently stronger interlayer bonding of dioctahedral minerals has not been determined. One possible explanation is that the smaller ionic radius of trivalent aluminum compared to divalent magnesium or iron would cause aluminum to form shorter, stronger ionic bonds [*Giese*, 1977]. A second possibility is that the octahedral cation charge in trioctahedral minerals is diluted by being spread over all three available sites, thereby weakening its effect on adjacent layers [*Giese*, 1978].

[24] The peak values of μ (dry) for the gouge samples are plotted against their calculated electrostatic separation energies in Figure 9. Because all the experiments were run at a constant effective normal stress of 100 MPa, all reported values of μ in this and Figures 3–5 correlate

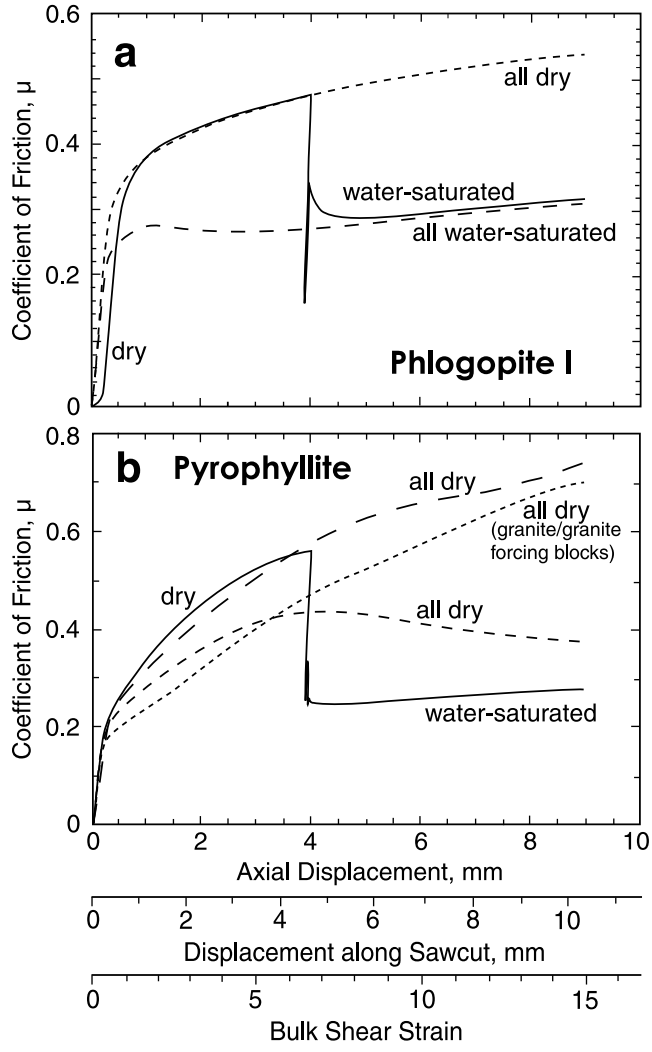

Figure 5. Comparison of dry/wet (solid lines) and all-dry friction experiments on (a) phlogopite I and (b) pyrophyllite gouges. An all-wet phlogopite experiment is also included in Figure 5a. Horizontal axes are the same as in Figure 3.

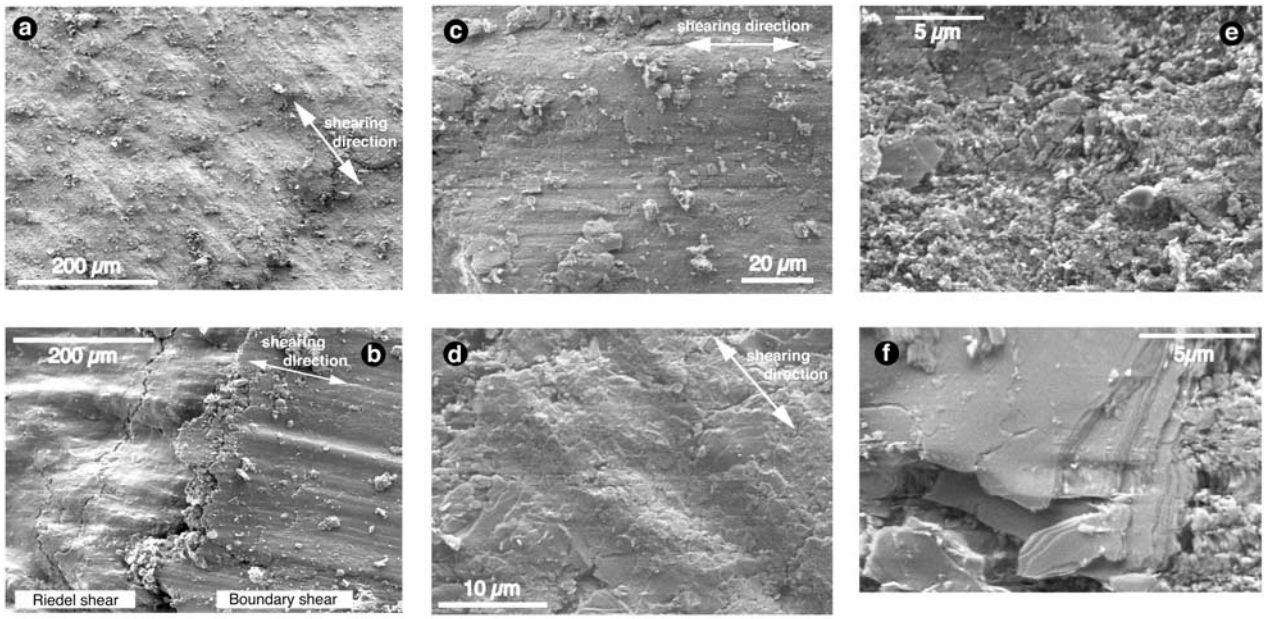

Figure 6. Secondary-electron SEM photomicrographs of shear surfaces developed in the gouge samples. (a) Boundary shear formed alongside the granite forcing block in an all-dry experiment on margarite gouge. Note the grainy, irregular surface and the short striations. (b) Intersection of boundary and R shears in graphite gouge from a dry/wet experiment. The R shear is lumpier than the boundary shear, but both surfaces are very shiny and striated. The R shear bends over to join the inner surface of the boundary shear. (c) Larger-scale and superposed smaller-scale striations on an R shear surface in a talc sample from an all-dry experiment. (d) Surface of striated boundary shear from the phlogopite I gouge sheared dry to 9-mm axial displacement, which shows the alignment of the platy grains parallel to the shear plane. (e) Close-up view of the margarite boundary shear in Figure 6a, on which platy grains are surrounded by fine-grained, more or less equigranular fragments. (f) Close-up of a crystal on a Riedel shear surface in the phlogopite I gouge from a dry/wet experiment. The layers appear to be progressively shifted to the left moving from the base to the top of the crystal.

directly with shear stress. Graphite was added to the plot at 0 separation energy, because the layers of covalently bonded carbon that constitute graphite are held together only by van der Waals forces (Figure 1). The range of μ (dry) found for pyrophyllite is indicated by the vertical arrow. Also included are the hardnesses measured on (001) [*Deer et al.*, 1962; *Mason and Berry*, 1968]. For these minerals the hardnesses measured on planes perpendicular to (001) are always higher than those measured on (001) [*Switzer*, 1941]. As seen in Figure 9, μ (dry) increases with increasing interlayer bond strength up to separation energies of $\approx$70 kcal/mol, which correspond to the (001) bond strengths of lizardite and gibbsite. For separation energies above this value, μ levels off at 0.80–0.85, consistent with Byerlee's Law. *Giese* [1978] did not calculate the bond strength of clintonite, but its strength is consistent with that of the other brittlemica, margarite. The three nonsilicate minerals in the 0–70 kcal/mol range are displaced toward slightly lower values of μ (dry) than the sheet silicates.

[25] We infer from Figure 9 that the average energy requirement associated with typical frictional processes in fault gouge, such as fracturing and abrasion, corresponds to $\approx$70 kcal/mol. For dry layer-structure minerals with interlayer bonds weaker than 70 kcal/mol, less energy is required to break those bonds than to initiate other frictional processes, and μ (dry) is directly correlated with the (001) bond strength. A similar correlation between dislocation glide energies of heated sheet silicates and interlayer bond strengths has also been noted [*Kronenberg et al.*, 1992; *Hickman et al.*, 1997].

[26] That the relationship between μ and interlayer bond strength can occur is due to the fact that shearing quickly becomes localized along boundary and R shears, and the platy minerals within the shears typically rotate until their (001) planes are oriented subparallel to the shear planes (Figures 6 and 7). This puts the grains into the best position for shear through the weak interlayer bonds. Similar alignments of sheet silicate minerals have been reported from many other laboratory shearing experiments [e.g., *Foster and De*, 1971; *Skempton*, 1985; *Will and Wilson*, 1989]. Naturally striated fault surfaces that are essentially identical to our laboratory samples have been described on the slip surfaces of landslides [*Skempton*, 1985] and on oceanic detachment faults whose surfaces are lined with chlorite, talc, and serpentine [*MacLeod et al.*, 2002]. The parallel arrangement of platy minerals under an applied load may embody the minimum free energy state [*Bolt*, 1956]. The spikes in μ measured near the beginning of the graphite experiments (Figure 3) and the broader, shallower peak in the water-saturated phlogopite I experiment (Figure 5a) may represent the work involved in rotating the grains.

[27] The streaks of biotite (Figure 7) and other weak minerals in these samples are direct evidence that the process of cleaving layered minerals during shear does

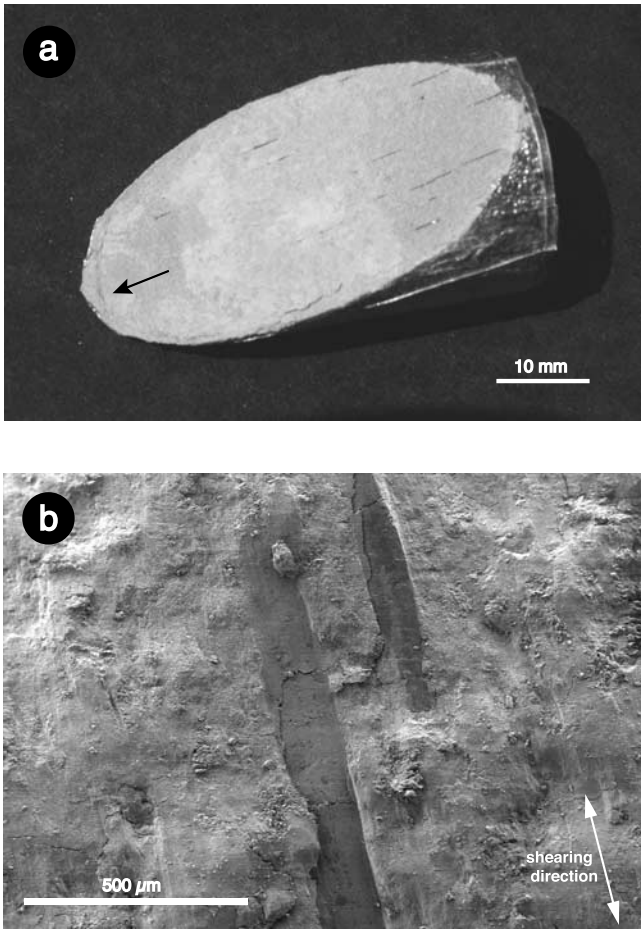

Figure 7. Biotite streaks in the phlogopite I gouge from a sample sheared dry to 9-mm axial displacement. (a) Series of streaks oriented parallel to the shear direction, viewed on the sandstone forcing block. (b) Secondary-electron SEM image of biotite streaks crossing the gouge layer along an R shear.

occur. As described previously, the biotite streaks form only in a gouge whose dry coefficient of friction equals or exceeds that of dry biotite. Talc, for instance, being considerably weaker than biotite, does not contain the biotite streaks. Where the streaks form, continued shear gradually thins the plates until the biotite in the streaks is barely distinguishable from the rest of the gouge. The interlayer bonds of margarite, clintonite, kaolinite, lizardite, and probably gibbsite are strong enough that they typically do not cleave during shear. Rather, as seen with margarite (Figures 6a and 6e), the plates break across (001) into small fragments during shear.

[28] The strength of dry pyrophyllite (Figure 5b) is correlated with the degree to which the gouge grains rotate into alignment with the shear planes (Figure 8). Why this rotation commonly is impeded for dry pyrophyllite is not known, although the grain shapes may be a factor. Many of the pyrophyllite grains have a bladed morphology. Instead of rotating in response to shear, such elongate grains may have preferentially formed kink bands or been bent and broken (Figure 8d). Given sufficient amounts of shear, the alignment of the dry pyrophyllite grains within the shear planes might increase, causing μ to decrease. Water-saturated pyrophyllite (Figures 4b and 5b) contains shear surfaces like those in Figure 8a [see also *Will and Wilson*, 1989], as do all the other water-saturated gouge samples.

[29] The role of adhesive forces between adjoining platy grains during dry shear could not be determined from petrographic examination of the gouge layers. However, numerous experimental studies [e.g., *Obreimoff*, 1930; *Bailey and Courtney-Pratt*, 1955] have demonstrated that when two mica (001) surfaces are brought into contact, they will adhere without the application of a load, and the adhesive contacts are sufficiently strong that the mica sheets can tear (cleave) upon separation [*Israelachvili and Adams*, 1976]. *Bailey and Courtney-Pratt* [1955] calculated a strength of nearly 10 Kg/mm^2 for shear between two plates of clean mica under normal loads and tangential forces $\leq$10 g weight and measured contact areas between $\approx$0.5 and 1.0×10^{-3} mm^2. Failure of the junctions between the mica sheets was always accompanied by the tearing of muscovite flakes from the surfaces. The numbers obtained by *Bailey and Courtney-Pratt* [1955] may not be directly applicable to our gouge experiments conducted at high normal stresses, but the damaged sample surfaces suggest that adhesive forces between mica plates are at least comparable to interlayer bonds of the crystals.

[30] *Giese* [1974, 1975a] converted the calculated separation energies for three minerals, muscovite, pyrophyllite, and talc, from units of kcal/mol to surface-energy units of J/m^2. Excluding graphite, all of the crystal structures described in Figure 1 are built on the same basic octahedral sheet exemplified by the minerals brucite and gibbsite, in which every 3 cation sites are filled either with 3 divalent cations (brucite) or 2 trivalent cations plus one vacancy (gibbsite). As a result, the *ab* lattice dimensions of all these minerals relative to a given number of octahedral cation sites are of closely comparable size. Accordingly, the other separation energies in Figure 9 were converted to units of J/m^2 assuming that *Giese* [1978] compared the same number of octahedral cation sites in all cases. This interpretation requires that the "molar" quantities of brucite and gibbsite used by *Giese* [1978] are $Mg_3(OH)_6$ and $Al_2(OH)_6$, respectively. The relative strengths of a dipole-dipole interlayer bond in brucite and of an interlayer hydrogen bond in lizardite, calculated by *Benco* [1997], are consistent with this interpretation.

[31] The minimum surface energies corresponding to Byerlee's Law would be about 2 J/m^2 (Figure 9). However, as mentioned previously, the electrostatic energy represents only a portion of the total interlayer bond strength. *Alcover and Giese* [1986] estimated the total (001) bond energy (consisting of the van der Waals, repulsion, and electrostatic energies) of talc, pyrophyllite, muscovite, and phlogopite. They compared two different models; one model would increase the surface energies reported in Figure 9 for these four minerals, on average, by about 0.2 J/m^2, the other would raise them by about 0.9 J/m^2. If the net increase for the two added energy terms is similar for all the sheet silicates, then attaining a coefficient of friction of 0.8 at 100 MPa effective normal stress would correspond to surface energies of either $\approx$2.2 J/m^2 or $\approx$2.9 J/m^2. It should be noted that the surface energies plotted in Figure 9 represent the cleavage energy, that is, the tensile strength

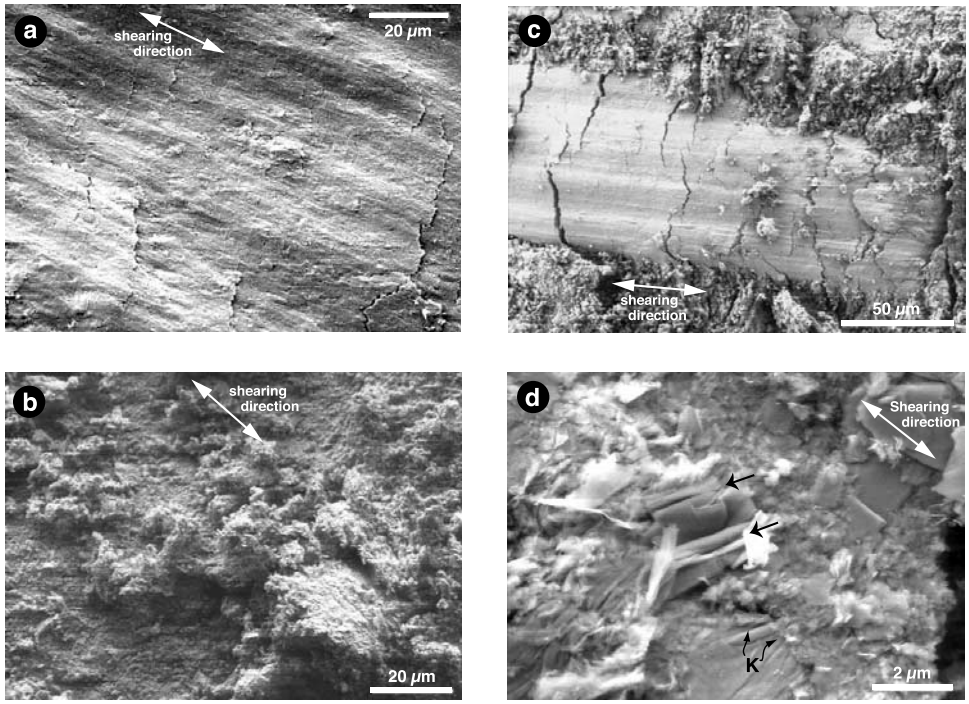

Figure 8. Textures in the all-dry pyrophyllite samples (Figure 5). (a) Weaker all-dry sample with smooth, shiny shear planes similar to those illustrated for graphite in Figure 6b. (b–d) Stronger all-dry samples. Figure 8b shows rough shear surface with little obvious parallel alignment of grains; Figure 8c shows local alignment of pyrophyllite grains to form a slickensided shear surface. The band of aligned grains is surrounded by unoriented gouge; Figure 8d shows close-up of a boundary shear, in which the (001) planes of some pyrophyllite grains are oriented parallel and others (marked by straight black arrows) perpendicular to the shear surface. Kink bands (K) have formed on one side of a parallel-oriented platelet.

of the (001) planes; these numbers may not correspond exactly to the shear strengths of those planes.

[32] Laboratory measurements of cleavage surface energies in sheet silicates have largely been restricted to muscovite and biotite/phlogopite, because these micas are the best sources of suitably large, good-quality crystals. The measured cleavage energies vary widely, depending on the conditions under which they were made. Natural micas cleaved under a high vacuum yield surface energies as high as 4.75 J/m^2 for muscovite [*Bryant*, 1962] and 3.63 J/m^2 for a natural phlogopite [*Gutshall et al.*, 1970]. A synthetic phlogopite cleaved by *Gutshall et al.* [1970] in a high vacuum was even stronger at 6.06 J/m^2. Cleavage energies measured in air at 1 atm on the same phlogopite samples were 0.5–0.7 J/m^2, much lower than in vacuum (and the natural phlogopite was stronger than the synthetic crystal). The 1-atm measurements are very close to the surface energy for phlogopite ($\approx$0.64 J/m^2) plotted in Figure 9. Most published tensile-fracture data for quartz and feldspars were also measured in ambient air conditions. The tensile-fracture surface energies for quartz that were included in the compilation of *Atkinson* [1984] vary between about 0.4 and 11.5 J/m^2, depending on the crystallographic plane that was broken and the experimental method used. The largest and smallest reported surface energies in this range, in fact, are for fracture of the same plane. Tensile-fracture surface energies for feldspars are more closely constrained between 3.2 and 7.8 J/m^2 [*Atkinson*, 1984]. The estimated 2–3 J/m^2 surface energy associated with the attainment of $\mu \approx 0.8$ is consistent with the feldspar fracture energies and also with the average of the quartz fracture energies.

[33] In summary, dry shear of layer-structure minerals with relatively weak (001) bonds (<70 kcal/mol electrostatic separation energy) occurs largely by breaking through the interlayer bonds to form new cleavage surfaces. For those minerals with stronger interlayer bonds ($\geq$70 kcal/mol), more energy is required to shear through the (001) plane than to initiate other frictional processes, and as a result those other frictional processes are dominant during dry shear.

4.2. Wet Friction

[34] Values of μ (wet) for these minerals are plotted relative to their calculated separation energies in Figure 10. Overall, wet friction increases with increasing separation energy, and some of the scatter in Figure 10 may occur because the different crystallographic groups are affected to different degrees by the addition of water (Figure 11). In general, the 2:1 sheet silicates have the smallest decreases in μ of $\leq$0.2 (Figure 11). Cleaving these minerals exposes the base of a tetrahedral sheet on both sides, with oxygen atoms at the surfaces. Wetting the two hydroxide minerals, brucite and gibbsite, produces a decrease in μ of 0.21–0.23, and cleaving these minerals separates two octahedral sheets with planes of hydroxyl ions at the surface. The 2:1 sheet silicate, chlorite was grouped with the 1:1 sheet silicates, because cleaving these minerals separates an octahedral sheet from

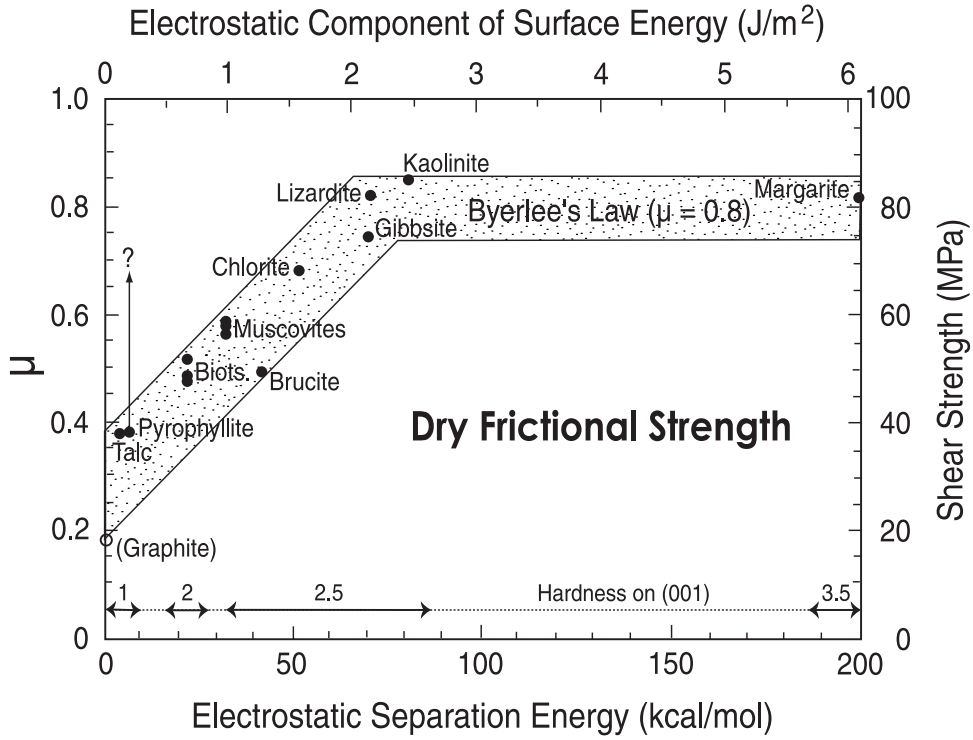

Figure 9. Peak values of μ (dry) plotted against calculated electrostatic separation energies [*Giese*, 1978, 1980; *Bish and Giese*, 1981] for those minerals, expressed on the lower axis in the units of kcal/mol reported in those papers and converted to units of J/m^2 on the upper axis (see text). Mineral hardnesses measured on (001), taken from *Deer et al.* [1962] and *Mason and Berry* [1968], are included for comparison. Because all values of μ (dry) were measured at constant 100 MPa normal stress, μ correlates directly with the shear stress supported by the gouge. The two muscovite data points and the (muscovite + paragonite) point are in a closely spaced group labeled muscovites; similarly, the phlogopite and biotite data are labeled biotites.

a tetrahedral sheet. For these three minerals, μ decreases by 0.3–0.4 with the addition of water. If each group of minerals in Figure 11 is considered individually in Figure 10, then μ increases regularly with increasing separation energy.

[35] The 2:1 sheet silicates comprise the largest group in this sample set, which allows some additional comparisons to be made. *Giese* [1978] concluded that layer charge and the nature of the octahedral sheet (whether dioctahedral or

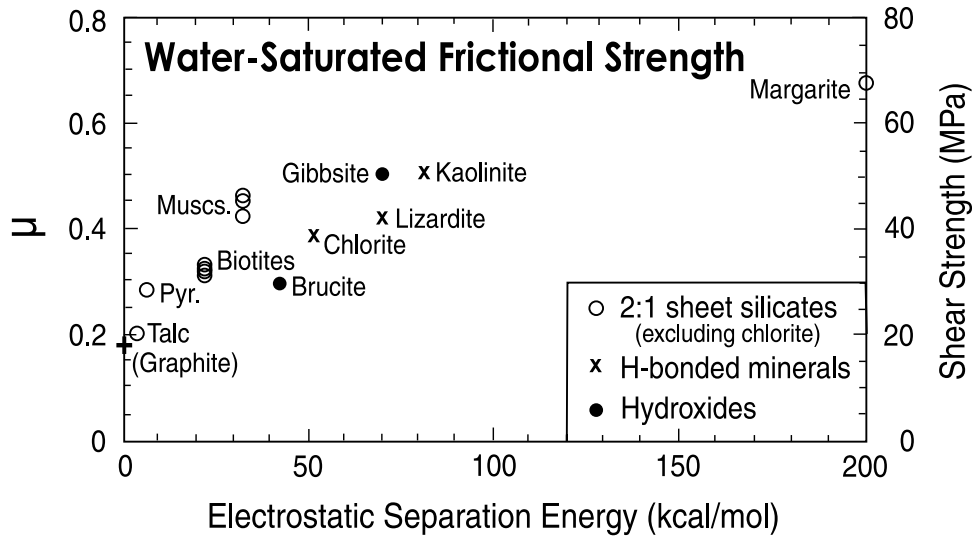

Figure 10. Relationships between water-saturated coefficients of friction and electrostatic separation energies [*Giese*, 1978, 1980; *Bish and Giese*, 1981]. Graphite strength is plotted (plus sign) at 0 kcal/mol electrostatic separation energy.

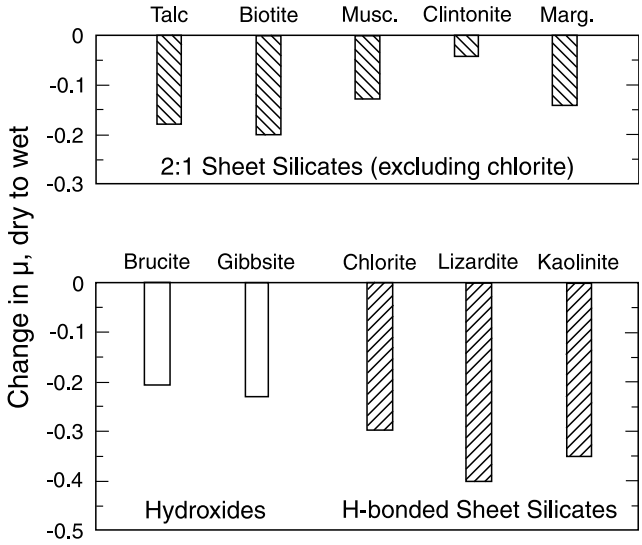

Figure 11. Bar graphs illustrating the decrease in μ accompanying the change from dry to water-saturated conditions during the strength experiments. Average values for the muscovite and biotite group data are plotted in Figure 11. Pyrophyllite was left off the top graph because of the questions about its dry strength. The amount of decrease is greatest for the minerals whose layers are held together by hydrogen bonds and is smallest, on average, for the micas and other 2:1 sheet silicates.

trioctahedral) were the major contributors to the interlayer bonds of 2:1 sheet silicates. Figure 12 compares μ (wet) with the charge on the tetrahedral sheets. Tetrahedral sheet charge was used instead of total layer charge, because it is the tetrahedral sheet that will come into contact with water. *Bleam* [1990] calculated that cation substitutions producing a charge imbalance in the octahedral sheet of pyrophyllite would contribute significantly less to the electrostatic potential of the (001) surface than equivalent substitutions in the tetrahedral sheet. *Sposito* [1984] reported that the bonding between water molecules and the basal oxygens of 2:1 sheet silicates is much stronger when the charge derives from tetrahedral substitutions [see also *Güven*, 1992]. The data for clintonite (Figure 4a) and montmorillonite [*Morrow et al.*, 2000] were included in Figure 12, and the data for the dioctahedral and trioctahedral minerals were fit with separate straight line trends. The coefficient of friction increases significantly with increasing tetrahedral sheet charge, and the dioctahedral minerals have larger values of μ than the trioctahedral ones for a given charge. The other two crystallographic groups (Figure 10) have similar relationships between dioctahedral and trioctahedral mineral strengths, kaolinite being stronger than lizardite and gibbsite being stronger than brucite.

[36] The water-saturated frictional strengths of these minerals can be explained in terms of the attraction of water molecules to the plate surfaces. As noted earlier, these gouges readily adsorb water from the surrounding air, and special care was needed to remove this water and keep it off during the dry-strength measurements. This surface-hydration force is quite strong, as demonstrated by experiments conducted by *Rutter* [1983] on kaolinite. A thin layer of kaolinite was compacted dry between two pistons under a 100 MPa uniaxial load. Once compaction was complete, a drop of water was added to the edge of the sample. The water was immediately taken up by the clay and the thickness of the clay layer increased against the applied load. The maximum amount of expansion was about twice as great at 50 MPa normal stress, which is consistent with the water film thicknesses calculated to be stable at those stress levels along flat grain-grain contacts [*Renard and Ortoleva*, 1997].

[37] It has been shown experimentally that water and other liquids form thin, structured films arranged in integral numbers of molecular layers when constrained between two

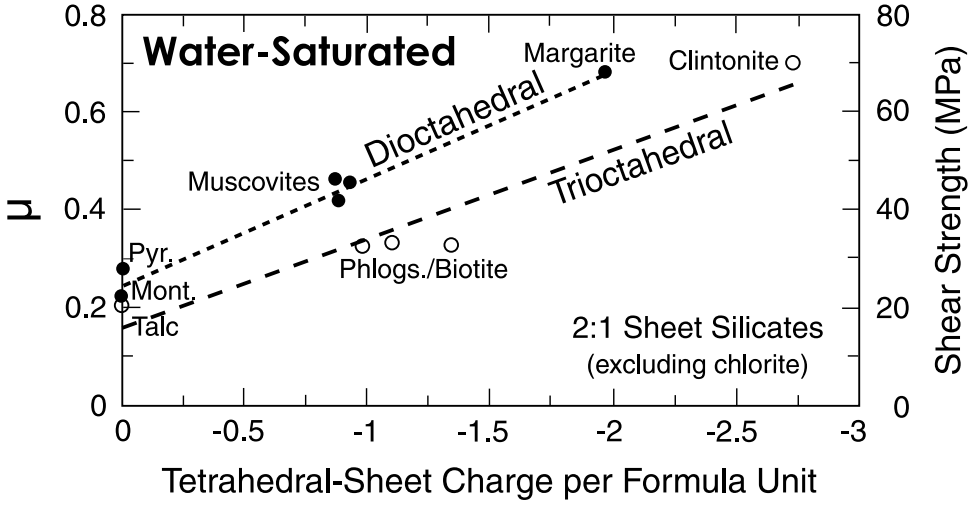

Figure 12. Correlation between water-saturated coefficient of friction and tetrahedral sheet charge of 2:1 layer silicates, including strength data for clintonite and montmorillonite. The tetrahedral sheet charge for the mixed muscovite + paragonite gouge is an average of their compositions (Table 1) weighted for their approximate modal abundances. Dashed lines are linear fits to the data for the dioctahedral (solid circles) and trioctahedral (open circles) minerals.

closely spaced mica sheets [*Israelachvili et al.*, 1988; *Homola et al.*, 1989]. This structuring occurs both laterally within a given water layer and across the thickness of the water film. These films have a shear strength that increases incrementally as the number of molecular layers in the film decreases [see also *Bailey and Courtney-Pratt*, 1955]. As was also suggested by *Rutter*'s [1983] experiments, the equilibrium number of layers comprising such a film decreases with increasing normal load. The calculations of *Renard and Ortoleva* [1997, Figure 4, p. 1968] indicate that the last remaining layer of water can withstand effective normal stresses as high as 800 MPa.

[38] The parallel alignment of the platy minerals in the shear planes of these gouge layers allows shear under water-saturated conditions to be concentrated in the water films that separate the plates. This is why the biotite streaks that formed during dry/wet experiments are shorter than those from all-dry experiments; once water is added to the gouge, shear is shifted from the interlayer planes of the biotite to the crystal surfaces. The measured variations in shear strength among the gouges (Figure 10) may reflect the strength of the bonding developed across the water layer and between the water and the different mineral surfaces. The positive correlations between μ and some of the factors that contribute to the (001) surface energy of layer-structure minerals, described above, suggest that in these high-pressure experiments the polar water molecules are bonded to the layer surfaces in proportion to the surface energies of the plates.

[39] The coefficient of wet friction of this group of minerals will be a complex function of the way a water molecule interacts with a given crystal surface. As illustrated by Figure 11, the amount of decrease from dry to wet μ differs for different structural groups. This may be a function of the type of bond that the water molecules make with different platy surfaces — whether the crystal surfaces are all tetrahedral sheets, all octahedral sheets, or a mix of the two. Preliminary modeling of the structure of interfacial water on layer-structure minerals indicates that water molecules will form different types of bonds with tetrahedral and octahedral surfaces [*Kalinichev et al.*, 2002]. This suggests, in turn, that the strength of a mixture of sheet structure minerals may depend, in part, on what sheets, tetrahedral and/or octahedral, form the surfaces of the crystals.

[40] Adding water to dry graphite gouge had no lubricating effect at the conditions tested (Figure 3). All solid surfaces attract water molecules, although the free energy of adhesion of water is lowest for apolar surfaces [*van Oss and Giese*, 1995] such as the graphite (001) plane. In light of the previous arguments, graphite frictional strength may be explained in one of two ways. One explanation is that the attraction of water to the covalently bonded carbon atoms on the graphite surfaces is low enough that a water film does not form at the normal stress conditions of these experiments. In that case the shear mechanism would be the same as for the dry samples. Alternatively, the water film is present, but in the absence of an electrostatic attraction to the mineral surfaces, the shear strength of the film is essentially the same as the van der Waals bonding between graphite layers.

[41] The montmorillonite data point in Figure 12 is also of interest. Montmorillonite is a dioctahedral smectite clay whose crystal structure is derived from that of pyrophyllite. The difference is that minor substitution in the octahedral sheet of montmorillonite is balanced by interlayer cations. Water molecules are attracted to the interlayer cations, and because the interlayer bonds are relatively weak, the water can enter the crystal structure causing the interlayer distance to increase ("swell"). Montmorillonite was one of the first very weak sheet silicate minerals identified, along with vermiculite [*Summers and Byerlee*, 1977a], a trioctahedral swelling clay that is similar to talc. Because both minerals are swelling clays, their low strengths were attributed to the generation of "pseudo pore pressures" [*Summers and Byerlee*, 1977a] as interlayer water was squeezed out of the crystals during shear, which was postulated to raise the pore fluid pressure and decrease the effective pressure [*Morrow et al.*, 1992]. However, the shear strength of montmorillonite is very close to the strengths of pyrophyllite and talc, neither of which takes on any interlayer water. As shown in Figure 12, μ of water-saturated montmorillonite is consistent with its crystallographic characteristics as a dioctahedral 2:1 sheet silicate. Thus the fact that montmorillonite is a swelling clay may be irrelevant to its frictional strength, and there is no need to invoke excess pore pressures or other special processes. The swelling properties of montmorillonite would be important only if the interlayer bond strength of the expanded crystal lattice were low enough that shear could as easily occur by cleaving the (001) planes as by shearing through the water films on the crystal surfaces. From the perspective of this study it is the high value of μ (dry) $\approx$0.7 for montmorillonite [*Morrow et al.*, 2000] that may require explanation. Because of the crystallographic similarities between montmorillonite and pyrophyllite, these two minerals may also behave similarly when sheared dry.

[42] The experiments of *Dieterich and Conrad* [1984] provide a possible analogue to the dry/wet experiments of this study. They ran direct-shear experiments on quartzite blocks to determine the effects of humidity on frictional strength. In experiments conducted at 1.7 MPa normal stress, the thoroughly dried quartzite had a coefficient of friction of 0.85–1.0, whereas the introduction of water reduced μ to 0.55–0.65. The flat block faces of the quartzite samples could perhaps be considered as rough approximations of platy mineral surfaces. Slicing through a quartz crystal breaks Si-O bonds, producing a surface charge [e.g., *Yates and Healy*, 1975; *Baudin et al.*, 1990] that attracts water [*Anderson and Wickersheim*, 1964; *Anderson*, 1965; see also *Parks*, 1984]. Shear of the wet quartzite blocks may thus have been concentrated in water films bonded to the quartz surfaces. The low normal stresses of their experiments would inhibit the formation of gouge during shear, which may be important because *Morrow et al.* [2000] found little change in μ during dry/wet experiments on quartz gouge. (The quartz gouge showed stick-slip motion under both dry and wet conditions, with wet shear at slightly higher average values of μ than dry shear [*Morrow et al.*, 2000].)

[43] If the mechanism of water-saturated friction described above for these minerals is correct, then the strength of the water films and, consequently, the shear strength should be affected by anything that modifies either the mineral surfaces or the properties of the fluid phase. One important factor is pore fluid chemistry, particularly the types and concentrations of cations present in solution [*Bolt*, 1956], and highly saline pore fluids have been shown to increase the strength of clay soils at low effective normal stresses [e.g., *Moore*, 1991;

Di Maio and Fenelli, 1994]. All of the experiments in this study were conducted on monomineralic gouges. A mixed sheet silicate gouge might yield unexpected results if the mixture combined minerals from different crystallographic groups (Figure 11). The physical interpretation of the slip-rate dependence of frictional strength in sheet silicate gouges also requires consideration of the crystal-water interface.

4.3. Implications of Dry and Wet Friction for Fault Zones

[44] The dry coefficient of friction may serve as an upper limit for the strength of the layer-structure minerals at depth in fault zones. As pressure increases, the water films separating the platy surfaces will become thinner, causing the strength to increase [*Rutter*, 1983; *Israelachvili et al.*, 1988; *Renard and Ortoleva*, 1997]. We have found that the strengths of illite-rich [*Moore et al.*, 1989] and serpentine-rich [*Moore et al.*, 1996b, 1997] gouges also increase with increasing temperature, but further study is needed to identify the cause or causes of the temperature-related increases. On the basis of the equations used by *Renard and Ortoleva* [1997] to calculate water film thickness, increasing temperature should have the opposite effect on gouge strength to increasing pressure. We interpreted the increase in μ of heated serpentine-mineral gouges along the lines of the oven-drying procedure used to prepare the dry gouge samples: Raising the temperature would tend to drive the adsorbed water off the mineral surfaces [*Moore et al.*, 1997]. Elevated temperatures will also activate a variety of processes that may promote the strengthening of fault gouge, and evidence for such processes should be sought in future investigations. Whatever the origin of the temperature effect, the strength of the heated gouge should never quite attain the dry friction value so long as it remains unlithified. Those layer-structure minerals with the weakest (001) bonds, such as talc, may thus be the best candidates to produce a mineralogically weak fault at seismogenic depths.

[45] A nominally dry friction experiment on a sheet structure mineral can yield very different results depending on room humidity, as demonstrated directly by *Reinen et al.* [1994] and indirectly by the wide range of numbers obtained from supposedly identical experiments. Unless there is a specific purpose for studying unsaturated gouge samples of clay or other sheet silicates, such as the oven-dried samples used for this study, any investigation that purports to have application to fault zones needs to be conducted under water-saturated conditions. This applies to all of the minerals in this group, but it is especially important for those minerals for which the difference between dry and water-saturated strength is large, such as the serpentine minerals and kaolinite (Figure 11). In addition, because the mechanisms of shear in dry and water-saturated sheet silicate gouges differ, the velocity dependence of their dry and water-saturated shear strengths may also differ.

5. Conclusions

[46] The relatively weak (001) interlayer bonds of sheet structure minerals govern their frictional strengths. With the possible exception of graphite, different shearing mechanisms are operative in thoroughly dried and water-saturated gouges of a given layer-structure mineral. The coefficient of dry friction increases from about 0.2 to 0.8 with increasing interlayer bond strength, with high friction coefficients corresponding to surface energies of 2–3 J/m^2. In this range, dry shear occurs by breaking through the interlayer bonds. The coefficient of friction levels off at 0.80–0.85 for minerals with stronger interlayer bonds, and other frictional processes dominate. This relationship occurs because shear is localized to boundary and Riedel shears, and the platy minerals within those shears rotate into alignment with the shear planes. The one apparent exception to this correlation is a gouge for which the parallel alignment of plates is suppressed and which, in consequence, is stronger than would be predicted from its interlayer bond strength.

[47] From previous work, we know that sheet structure minerals attract water to their surfaces and the water forms thin, structured films between adjacent platy grains even under high effective normal stresses. The strength of the bonding between the water and the mineral surfaces increases with the strength of the mineral's interlayer bonds, although the nature of the plate surfaces is also important. The results of this study can be explained if shear of water-saturated gouges is controlled by thin water films that require higher stresses to shear through when they are bonded strongly to sheet structure minerals. At the experimental conditions tested, the frictional strength of the swelling clay montmorillonite can be explained completely in terms of shear through the water films at the plate surfaces, without the need to invoke special behavior associated with its swelling properties.

[48] With increasing effective pressure and temperature the coefficients of friction of several of these gouges have been shown to increase toward the dry values, although further study is needed to determine the cause of the temperature effect. The dry strength can therefore be used to estimate the peak strength of a sheet structure mineral at seismogenic depths.

Appendix A: Sample Descriptions

A1. Graphite

[49] A commercial graphite powder (grade #38) from Fisher Scientific was used in this study. It required no sample preparation.

A2. Brucite

[50] The brucite starting material consists of clear, colorless, lamellar crystals from Lancaster County, Pennsylvania, obtained from Ward's Scientific. Inclusions of a carbonate mineral and a dark-green sheet silicate were removed before grinding. This same separate was used by *Moore et al.* [2001].

A3. Gibbsite

[51] The gibbsite separate was prepared from botryoidal masses of gibbsite from Minas Gerais, Brazil, that were obtained from Mineralogical Research Co. of San Jose, California.

A4. Lizardite

[52] Samples of a lizardite-rich, serpentinized peridotite (>90% serpentine minerals) from Gold Beach, Oregon,

were provided by R. G. Coleman. Bluish-green veins of serpentine and blue-green altered rock, suspected of being chrysotile, were removed before grinding. The lizardite is the common 1T polytype. This mineral separate was also used by *Moore et al.* [1997].

A5. Kaolinite

[53] Kaolinite of probable hydrothermal origin was collected at outcrops near Mammoth Lake, California. The sample underwent no treatment other than sieving. The XRD pattern shows no traces of impurities, but a few small grains of quartz are visible in thin section.

A6. Talc

[54] The talc sample is a commercial, purified-grade talcum powder of end-member composition from Fisher Scientific. The talc required no preparation for use.

A7. Pyrophyllite

[55] The starting material comes from Hillsboro, North Carolina (Ward's Scientific), and it consists of acicular sprays of pyrophyllite crystals, averaging 5 mm in length, that sit on a matrix of fine-grained pyrophyllite and quartz. The larger crystals were preferentially selected for the mineral separate. The XRD pattern corresponds to the 2M variety.

A8. Montmorillonite

[56] The montmorillonite sample is a commercial product, Volclay MPS-1 from American Colloid Company, whose chemical analysis yields the mineral formula: $Na_{0.3}(Fe^{+2}, Mg)_{0.3}(Al,Fe^{+3})_{1.7}Si_4O_{10}(OH)_2 \cdot nH_2O$. It required no preparation for use.

A9. Muscovite I

[57] The source material was a large, brownish-gray crystal obtained from the California Academy of Sciences in San Francisco. The entire crystal had been crushed and ground for use by *Summers and Byerlee* [1977a, 1977b]. Because the mica flakes were coarser-grained than the others used for this study, a portion of the prepared gouge was reground and sieved for these experiments. The XRD pattern is consistent with the $2M_1$ polytype.

A10. Muscovite II

[58] The crystal selected for the separate was a large, light-brown crystal from Stoneham, Maine (Ward's Scientific), that was generally free of inclusions. Sample preparation consisted of removing weathered edges before grinding. The XRD pattern fits the $2M_1$ polytype.

A11. Paragonite + Muscovite

[59] The starting material is a paragonite-bearing muscovite schist from Chester, Vermont (Ward's Scientific), in which thin, mica-rich layers alternate with quartz-rich layers. The paragonite and muscovite are indistinguishable under the stereomicroscope, which precluded effective separation of the two minerals. SEM and XRD examinations indicate that the muscovite is somewhat more abundant than the paragonite both in the rock specimen and the mineral separate.

A12. Biotite

[60] Large, black crystals from Bancroft, Ontario (Ward's Scientific), provided the source material for this separate. The mineral is biotite based on its black color, but the Fe/Mg ratio is sufficiently low to classify it chemically as phlogopite (see discussion of phlogopite/biotite terminology by *Deer et al.* [1962, p. 42]). The high fluorine content of this mica (4.7 wt % F) represents replacement of about half the (OH) sites by F. The XRD pattern matches the 1M polytype. Sample preparation largely involved removal of weathered surfaces. The E-series biotite of *Noe et al.* [1999] and the biotite studied by *Kronenberg et al.* [1990] also come from Bancroft, Ontario.

A13. Phlogopite I

[61] The separate was prepared from large, brownish-gray crystals from Quebec (Ward's Scientific). The XRD pattern fits a 3T polytype. Coatings on some of the cleavage surfaces and inclusions of opaque minerals were removed prior to grinding.

A14. Phlogopite II

[62] This phlogopite sample comes from a phlogopite-rich schist from Little Butte, east Helena, Montana (Ward's Scientific). The phlogopite occurs as light-green crystals up to 1 cm in diameter, allowing for easy separation from minerals such as magnetite. The XRD pattern is consistent with a 3T variety.

A15. Clintonite

[63] The clintonite separate was derived from a rock sample containing clintonite + vesuvianite + calcite from Crestmore quarry, Riverside County, California (Mineralogical Research Co.). The XRD pattern most closely matches the 1M variety.

A16. Margarite

[64] Clear, pale-pink crystals of margarite up to 1 cm in diameter dominate this rock sample from Chester, Massachusetts (Ward's Scientific). Some chlorite is also present, but the two sheet silicates generally occur separately. The composition listed in Table 1 is very similar to a wet-chemical analysis of margarite from the same locality [*Deer et al.*, 1962, p. 97].

A17. Chlorite

[65] The medium-grained, deep-green chlorite comprising this separate is a ripidolite [*Hey*, 1954] derived from a chlorite-garnet schist from Flagstaff Hill, California. The source materials for this study were the unused wafers that had been prepared for a series of strength experiments by *Summers and Byerlee* [1977a, 1977b]. The wafers were broken up, and the garnets were removed prior to grinding.

References

Alcover, J. F., and R. F. Giese (1986), Energie de liaison des feuillets de talc, pyrophyllite, muscovite, et phlogopite, *Clay Miner.*, *21*, 159–169.

Anderson, J. H. (1965), Calorimetric vs. infrared measures of adsorption bond strength in silica, *Surf. Sci.*, *3*, 290–291.

Anderson, J. H., Jr., and K. A. Wickersheim (1964), Near infrared characterization of water and hydroxyl groups on silica surfaces, *Surf. Sci.*, *2*, 252–260.

Atkinson, B. K. (1984), Subcritical crack growth in geological materials, *J. Geophys. Res.*, *89*, 4077–4114.

Bailey, A. I., and J. S. Courtney-Pratt (1955), The area of real contact and the shear strength of monomolecular layers of a boundary lubricant, *Proc. R. Soc. London A*, *227*, 500–515.

Baudin, I., A. Ricard, and R. Audebert (1990), Adsorption of dextrans and pollulans at the silica-water interface; hydrodynamic layer thickness measurements; role in the fouling of ultrafiltration membranes, *J. Colloid Interface Sci.*, *138*, 324–331.

Benco, L. (1997), Electron densities in hydrogen bonds: Lizardite-1*T*, *Eur. J. Mineral.*, *9*, 811–819.

Bish, D. L., and R. F. Giese Jr. (1981), Interlayer bonding in IIb chlorite, *Am. Mineral.*, *66*, 1216–1220.

Bleam, W. F. (1990), The nature of cation-substitution sites in phyllosilicates, *Clays Clay Miner.*, *38*, 527–536.

Bolt, G. H. (1956), Physico-chemical analysis of the compressibility of pure clays, *Geotechnique*, *6*, 86–93.

Bryant, P. J. (1962), Cohesion of clean surfaces and the effect of adsorbed gas, in *Transactions Ninth National Vacuum Symposium*, edited by G. H. Bancroft, pp. 311–313, Macmillan, New York.

Byerlee, J. D. (1978), Friction of rocks, *Pure Appl. Geophys.*, *116*, 615–626.

Deer, W. A., R. A. Howie, and J. Zussman (1962), *Rock-Forming Minerals*, vol. 3, *Sheet Silicates*, 270 pp., John Wiley, Hoboken, N. J.

Dieterich, J. H., and G. Conrad (1984), Effect of humidity on time- and velocity-dependent friction in rocks, *J. Geophys. Res.*, *89*, 4196–4202.

Di Maio, C., and G. B. Fenelli (1994), Residual strength of kaolin and bentonite: The influence of their constituent pore fluid, *Geotechnique*, *44*, 217–226.

Foster, R. H., and P. K. De (1971), Optical and electron microscopic investigation of shear induced structures in lightly consolidated (soft) and heavily consolidated (hard) kaolinite, *Clays Clay Miner.*, *19*, 31–47.

Giese, R. F., Jr. (1973), Interlayer bonding in kaolinite, dickite, and nacrite, *Clays Clay Miner.*, *21*, 145–149.

Giese, R. F., Jr. (1974), Surface energy calculations for muscovite, *Nature*, *248*, 580–581.

Giese, R. F., Jr. (1975a), Interlayer bonding in talc and pyrophyllite, *Clays Clay Miner.*, *23*, 165–166.

Giese, R. F., Jr. (1975b), The effect of F/OH substitution on some layer-silicate minerals, *Z. Kristallogr.*, *141*, 138–144.

Giese, R. F., Jr. (1977), The influence of hydroxyl orientation, stacking sequence, and ionic substitutions on the interlayer bonding of micas, *Clays Clay Miner.*, *25*, 102–104.

Giese, R. F., Jr. (1978), The electrostatic interlayer forces of layer structure minerals, *Clays Clay Miner.*, *26*, 51–57.

Giese, R. F., Jr. (1980), Hydroxyl orientations and interlayer bonding in amesite, *Clays Clay Miner.*, *28*, 81–86.

Gutshall, P. L., P. J. Bryant, and G. M. Cole (1970), Cleavage surface energy of phlogopite mica, *Am. Mineral.*, *55*, 1432–1434.

Güven, N. (1992), Molecular aspects of clay/water interactions, in *Clay-Water Interface and its Rheological Implications*, edited by N. Güven and R. M. Pollastro, *Clay Min. Soc. Workshop Lect.*, *4*, 1–79.

Hey, M. H. (1954), A new review of the chlorites, *Mineral. Mag.*, *30*, 277–292.

Hickman, J. B., E. N. Zhurina, and A. K. Kronenberg (1997), Deformation of talc and pyrophyllite: Disruption of van der Waals bonds and comparisons with calculated interlayer forces (abstract), *Eos Trans AGU*, *78*(46), Fall Meet. Suppl., F724.

Homola, A. M., J. N. Israelachvili, M. L. Gee, and P. M. McGuiggan (1989), Measurement of and relation between the adhesion and friction of two surfaces separated by molecularly thin liquid films, *J. Tribol.*, *111*, 675–682.

Israelachvili, J. N., and G. E. Adams (1976), Direct measurement of long range forces between two mica surfaces in aqueous KNO_3 solutions, *Nature*, *262*, 774–776.

Israelachvili, J. N., P. M. McGuiggan, and A. M. Homola (1988), Dynamic properties of molecularly thin liquid films, *Science*, *240*, 189–191.

Kalinichev, A. G., R. T. Cygan, J. Wang, and R. J. Kirkpatrick (2002), Structure and dynamics of mineral/water interfaces: Molecular dynamics simulations of clays and clay-related phases, *Eos Trans AGU*, *83*, Fall Meet. Suppl., Abstract V51A-1233.

Kronenberg, A. K., S. H. Kirby, and J. Pinkston (1990), Basal slip and mechanical anisotropy of biotite, *J. Geophys. Res.*, *95*, 19,257–19,278.

Kronenberg, A. K., V. M. Mares, and R. G. Christoffersen (1992), Deformation of micas: Easy glide and effects of crystal chemistry and structure on (001) dislocation motion (abstract), *Eos Trans. AGU*, *73*, Fall Meet. Suppl., 528.

Mackenzie, R. C., ed. (1957), *The Differential Thermal Analysis of Clays*, 456 pp., Mineral. Soc., London.

MacLeod, C. J., et al. (2002), Direct geological evidence for oceanic detachment faulting: The Mid-Atlantic Ridge, 15°45′N, *Geology*, *30*, 879–882.

Mason, B., and L. G. Berry (1968), *Elements of Mineralogy*, 550 pp., W. H. Freeman, New York.

Moore, D. E., R. Summers, and J. D. Byerlee (1989), Sliding behavior and deformation textures of heated illite gouge, *J. Struct. Geol.*, *11*, 329–342.

Moore, D. E., D. A. Lockner, R. Summers, J. D. Byerlee, and S. Ma (1996a), Sample characterizations and strength measurements of serpentinite gouges, *U.S. Geol. Surv. Open File Rep.*, *96-702*, 88 pp.

Moore, D. E., D. A. Lockner, R. Summers, S. Ma, and J. D. Byerlee (1996b), Strength of chrysotile-serpentinite gouge under hydrothermal conditions: Can it explain a weak San Andreas fault?, *Geology*, *24*, 1041–1044.

Moore, D. E., D. A. Lockner, S. Ma, R. Summers, and J. D. Byerlee (1997), Strengths of serpentinite gouges at elevated temperatures, *J. Geophys. Res.*, *102*, 14,787–14,801.

Moore, D. E., D. A. Lockner, K. Iwata, H. Tanaka, and J. D. Byerlee (2001), How brucite may affect the frictional properties of serpentinite, *U.S. Geol. Surv. Open File Rep.*, *01–320*, 14 pp.

Moore, R. (1991), The chemical and mineralogical controls upon the residual strength of pure and natural clays, *Geotechnique*, *41*, 35–47.

Morrow, C., B. Radney, and J. Byerlee (1992), Frictional strength and the effective pressure law of montmorillonite and illite clays, in *Fault Mechanics and Transport Properties of Rocks*, edited by B. Evans and T.-F. Wong, pp. 69–88, Academic, San Diego, Calif.

Morrow, C. A., D. E. Moore, and D. A. Lockner (2000), The effect of mineral bond strength and adsorbed water on fault gouge frictional strength, *Geophys. Res. Lett.*, *27*, 815–818.

Noe, D. C., D. A. LaVan, and D. Veblen (1999), Lap shear testing of biotite and phlogopite crystals and the application of interferometric strain/displacement gages to mineralogy, *J. Geophys. Res.*, *104*, 17,811–17,822.

Obreimoff, J. W. (1930), The splitting strength of mica, *Proc. R. Soc. London A*, *127*, 290–297.

Parks, G. A. (1984), Surface and interfacial free energies of quartz, *J. Geophys. Res.*, *89*, 3397–4008.

Reinen, L. A., J. D. Weeks, and T. E. Tullis (1994), The frictional behavior of lizardite and antigorite serpentinites: Experiments, constitutive models, and implications for natural faults, *Pure Appl. Geophys.*, *143*, 317–358.

Renard, F., and P. Ortoleva (1997), Water films at grain-grain contacts: Debye-Hückel, osmotic model of stress, salinity, and mineralogy dependence, *Geochim. Cosmochim. Acta*, *61*, 1963–1970.

Rutter, E. H. (1983), Pressure solution in nature, theory, and experiment, *J. Geol. Soc. London*, *140*, 725–740.

Skempton, A. W. (1985), Residual strength of clays in landslides, folded strata and the laboratory, *Geotechnique*, *35*, 3–18.

Sposito, G. (1984), *The Surface Chemistry of Soils*, 234 pp., Oxford Univ. Press, New York.

Stanchits, S. A., D. A. Lockner, and A. V. Ponomarev (2003), Anisotropic changes in P-wave velocity and attenuation during deformation and fluid infiltration of granite, *Bull. Seismol. Soc. Am.*, *93*, 1803–1822.

Summers, R., and J. Byerlee (1977a), A note on the effect of fault gouge composition on the stability of frictional sliding, *Int. J. Rock Mech. Min. Sci.*, *14*, 155–160.

Summers, R., and J. Byerlee (1977b), Summary of results of frictional sliding studies, at confining pressures up to 6.98 kb, in selected rock materials, *U.S. Geol. Surv. Open File Rep.*, *77-142*, 129 pp.

Switzer, G. (1941), Hardness of micaceous minerals, *Am. J. Sci.*, *239*, 316.

van Oss, C. J., and R. F. Giese (1995), The hydrophilicity and hydrophobicity of clay minerals, *Clays Clay Min.*, *43*, 474–477.

Will, T. M., and C. J. L. Wilson (1989), Experimentally produced slickenside lineations in pyrophyllitic clay, *J. Struct. Geol.*, *11*, 657–667.

Yates, D. E., and T. W. Healy (1975), The structure of the silica/electrolyte interface, *J. Colloid Interface Sci.*, *55*, 9–19.

Zhang, S., T. E. Tullis, and V. J. Scruggs (2001), Implications of permeability and its anisotropy in a mica gouge for pore pressures in fault zones, in *Deformation Processes in the Earth's Crust*, edited by J. Boland and A. Ord, *Tectonophysics*, *335*, 37–50.

D. A. Lockner and D. E. Moore, U. S. Geological Survey, Mail Stop 977, 345 Middlefield Road, Menlo Park, CA 94025, USA. (dmoore@usgs. gov)